Green Chemistry

A Facile Strategy for Photoactive Nanocellulose-based Antimicrobial Materials

Journal:	*Green Chemistry*
Manuscript ID	GC-ART-02-2019-000551.R2
Article Type:	Paper
Date Submitted by the Author:	17-May-2019
Complete List of Authors:	Alvarado, David; North Carolina State University, Department of Chemistry Argyropoulos, D. S.; North Carolina State University , Forest Biomaterials Scholle, Frank; North Carolina State University, Department of Biological Sciences Peddinti, Bharadwaja ; North Carolina State University, Department of Chemical and Biomolecular Engineering Ghiladi, Reza; North Carolina State University, Department of Chemistry

Green Chemistry

ARTICLE

A Facile Strategy for Photoactive Nanocellulose-based Antimicrobial Materials

+Received 00th January 20xx,
Accepted 00th January 20xx

DOI: 10.1039/x0xx00000x

www.rsc.org/

David Ramirez Alvarado,[a] Dimitris S. Argyropoulos,[b] Frank Scholle[c], Bharadwaja S.T. Peddinti[d] and Reza A. Ghiladi [a]*

The prolonged survival of microbes on surfaces in high-traffic/high-contact environments drives the need for a more consistent and passive form of surface sterilization, with the goal of minimizing pathogen transmission. Here, we developed self-disinfecting materials through the covalent attachment of a porphyrin-based photosensitizer (PS) to nanofibrillated cellulose (NFC) and paper (Pap), imparting antimicrobial activity to these renewable scaffolds via photodynamically generated singlet oxygen. The facile covalent attachment of the free-base 5-(4-aminophenyl)-10,15,20-tris-(4-N-methylpyridinium)porphyrin (A_3B^{3+}) and metallated [5-(4-aminophenyl)-10,15,20-tris-(4-N-methylpyridinium)porphyrinato]zinc(II) (Zn-A_3B^{3+}) photosensitizers was accomplished by aqueous cyanuric chloride coupling, avoiding the use of organic solvents of previous coupling strategies, while preventing PS leaching that is an issue with non-covalent PS incorporation strategies. Materials characterization and the degree of photosensitizer loading were determined by FTIR, elemental and TGA analyses, and UV-Visible Diffuse Reflectance Spectroscopy (UV-Vis DRS). The antimicrobial potencies of the resultant PS-NFC and PS-Pap materials were evaluated against four strains of bacteria recognized by the World Health Organization as either critical or high priority pathogens: Gram-positive strains methicillin-resistant *S. aureus* (MRSA; ATCC-44) and vancomycin-resistant *E. faecium* (VRE; ATCC-2320), and Gram-negative strains multidrug-resistant *A. baumannii* (MDRAB; ATCC-1605) and NDM-1 positive *K. pneumoniae* (KP; ATCC-2146). Our results demonstrated broad photodynamic inactivation of all strains studied upon illumination (30 min; 65±5 mW/cm^2; 400-700 nm) by a minimum of 99.999%. Antiviral studies against two enveloped viruses, dengue-1 (DENV) and vesicular stomatitis virus (VSV), revealed complete inactivation by both materials. Taken together, the results demonstrate the potential for photoactive NFC as the basis for sustainable broad spectrum anti-infective materials.

Introduction

Nosocomial infections have increasingly attracted much attention due to the dwindling efficacy of antibiotics against culprit pathogenic microorganisms.[1] In 2017, the World Health Organization (WHO) released a list of “HIGH” and “CRITICAL” priority Gram-positive and Gram-negative bacterial pathogens demanding a global effort towards the advancement of antibiotics.[2] The origin of infection proliferation lies in the ease with which these pathogens are transmitted, not just directly from the healthcare worker to the patient, but also indirectly from the hospital environment: the survival of nosocomial pathogens, including *Acinetobacter baumannii* and *Staphylococcus aureus*, has been documented to range from weeks to months on inanimate surfaces.[3, 4] Bacterial resilience, combined with the rapid evolutionary acquisition of antibiotic resistance, makes the development of combative strategies crucial. Among these, efforts to minimize nosocomial pathogen transfer have emerged in the form of antimicrobial textile research with a targeted approach being passive disinfection.[5-11] Ideally, such textiles and/or surfaces should possess outstanding cytotoxic characteristics, excellent tolerances for repeated human contact, and be based on naturally occurring materials derivatized with minimal environmental impact.

For these reasons, significant attention has been paid in the literature on cellulose as being the basis for such materials.[12, 13] Cellulose is the most abundant organic biopolymer on the planet, possessing easily accessible hydroxyl groups located along its repeating anhydroglucose ring, providing ample sites for functionalization and/or covalent incorporation of microbicidal agents.[14, 15] While chemical grafting and embedment are both proven methods for the inclusion of biocidal agents,[16-23] the preference lies, however, in the immobilization of the microbicide due to obvious environmental concerns in case of possible prolonged leaching, and to maintain material efficacy. Recently, efforts to conjugate a multitude of antimicrobial agents to cellulose have

---

[a] *Department of Chemistry, North Carolina State University, 2620 Yarbrough Drive, Raleigh, North Carolina 27695, USA*
[b] *Department of Forest Biomaterials, North Carolina State University, 2820 Faucette Drive, Raleigh, North Carolina 27695, USA*
[c] *Department of Biological Sciences, North Carolina State University, 112 Derieux Place, Raleigh, North Carolina 27695, USA*
[d] *Department of Chemical & Biomolecular Engineering, North Carolina State University, 911 Partners Way, Raleigh, North Carolina 27695, USA*

Electronic Supplementary Information (ESI) available: Antimicrobial activity and singlet oxygen quantum yield studies of PS **3** and **4**. See DOI: 10.1039/x0xx00000x been successful, including the attachment of silanes, antibiotics, chlorins, and quaternary ammonium salt-chromophore conjugates, among others.[24-27] As such, cellulose-based antimicrobial materials have the potential for a considerable array of end use applications,[28] including surface coatings or personal protective equipment in the healthcare environment. Likewise, any industry or setting that benefits from the absence of pathogen contamination is also a candidate.

Because of the potential for antimicrobial material adoption across multiple industries, it is at this stage at which the science and engineering must be optimized for maximum performance and minimum environmental impact. Here, we describe the development of a cellulose-based antimicrobial material using three components: i) a nanofibrillated cellulose (NFC) scaffold, ii) a triazine linker, and iii) a photosensitizer for photodynamic inactivation of bacteria. The rationale behind each is as follows:

i) Nanofibrillated Cellulose (NFC): The use of nanofibrillated cellulose has seen relatively limited attention for application in antimicrobial materials,[29] specifically covalent functionalization of cytotoxic agents.[30-35] Key features that advocate its use include its renewable nature, the ease of surface functionalization, and high aspect and surface area-to-volume ratios – the specific surface area of a single gram of NFC can range as high as 50 to 70 m^2, making this material an excellent candidate for the development of textiles, surface coatings and an assortment of other applications.[14]

ii) Triazine Linker: Our earlier work used the Cu(I)-catalyzed Huisgen-Meldal-Sharpless 1,3-dipolar cycloaddition, a "click" reaction, to covalently couple porphyrin photosensitizers to cellulosic substrates.[16-18] While this method was successful, this protocol is both cumbersome and environmentally unsustainable: drawbacks include a number of pre-treatment steps at elevated temperatures for both the cellulose scaffold and the photosensitizer, the need for a metal-based catalyst, and is limited to synthetic photosensitizers. Inspired by the earlier work of Sol and co-workers,[19, 20] we have chosen 2,4,6-trichloro-1,3,5-triazine (otherwise known as cyanuric chloride) for the covalent attachment of photosensitizers to cellulose.[36] Substitution of the chlorine atoms with nucleophiles such as amines, phenols, and thiols is facile, proceeds under mild conditions, requires no metal-based catalyst, and with reasonable atom economy.[37-40] Covalent coupling of the PS also prevents its leaching into the environment that is a drawback of non-covalent (electrostatic or embedding) strategies.

iii) Photosensitizer for aPDI: The mode of operation behind antimicrobial photodynamic inactivation (aPDI) is the generation of highly reactive singlet oxygen ($^1O_2$) and other reactive oxygen species (ROS) upon illumination of a photosensitizer.[41] The ability of singlet oxygen to react indiscriminately against a variety of microbes (including both Gram-positive and -negative bacterial species, viruses with capsid or lipid envelopes, fungi/yeasts, and mycobacteria) makes this approach of inactivation highly attractive,[42-47] particularly for antimicrobial applications involving photoactive nanomaterials.[48-51] Moreover, aPDI is equally effective against pathogens that are resistant to conventional antibiotics when compared with their drug-susceptible counterparts, and resistance to singlet oxygen is believed to be unlikely.[52-55] Importantly, given the short half-life of singlet oxygen (2 μs) that leads to its limited diffusibility in solution (<250 nm),[56, 57] and the fact that it decays back to harmless, breathable O_2 all together make the use of singlet oxygen an environmentally benign, yet potent microbicidal agent.

Given the above considerations, we have developed photosensitizer (PS) linked nanofibrillated cellulose (PS-NFC) and paper sheets (PS-Pap) via the covalent attachment of a porphyrin-based photosensitizer using a triazine linker methodology. While we selected a synthetic porphyrin-based photosensitizer here to allow for comparisons to previously studied materials,[16-18, 58, 59] we note that this strategy can be easily extended to naturally occurring photosensitizers (i.e., PPIX,[60, 61] hypocrellin,[62] curcumin,[63] etc.). The surface modification of the nanofibrillated cellulose scaffold was accomplished under relatively mild conditions where recovery of solvent and reagents is feasible, thus lessening environmental impact. As will be shown, the PS-NFC and PS-Pap materials were highly effective in the photodynamic inactivation of drug-resistant Gram-positive and -negative bacteria, as well as two viruses, and suggests that the methodology described below can be a general route for the development of potent antimicrobial materials based on a nanocellulose scaffold.

Experimental

Materials

Nanofibrillated cellulose (NFC) was provided by Stora Enso Corporation as an aqueous suspension containing 5.35±0.04 wt% of solid polysaccharide. VWR qualitative grade 415 filter paper was used as the source of cellulose for the photosensitizer-paper conjugate materials. All reagents and solvents were purchased from commercial sources and used as received unless otherwise noted. Flash chromatography utilized Agela Technologies Flash Silica Gel (40-60 μm mesh, 60 Å). Nutrient broths and agar for the culturing of bacteria were purchased from commercial vendors (Tryptic Soy Broth, BD Difco Nutrient Broth #234000, and BD Difco Bacto Brain Heart Infusion #237500 from BD Biosciences; LB-Media from Teknova; agar from Hardy Diagnostics).

Instrumentation

^{1}H-NMR spectra were acquired using Varian Mercury 300 or 400 MHz spectrometers utilizing TMS as an internal standard. UV-visible spectra were acquired on a Varian Cary Bio50 spectrophotometer or a Shimadzu UV-3600 spectrophotometer. Mass spectrometry analyses were made in the Molecular Education, Technology, and Research Innovation Center (METRIC) at NC State University carried out on an AB Sciex 5800 MALDI-TOF/TOF MS or on a Bruker Daltonics autoflex maX MALDI-TOF MS in the absence of a matrix. Ultra-high resolution scanning electron microscopy (SEM) images were collected on an FEI Verios 460L field-emission scanning electron microscope. Diffuse reflectance UV-Vis (DR-UV-Vis) spectroscopy was conducted on a Shimadzu UV-Vis-NIR Spectrophotometer UV-3600 in the wavelength range of 300 to 800 nm. Fourier transform infrared spectra were acquired on an IR-Prestige 21 Shimadzu Fourier Transform Infrared Spectrophotometer equipped with a GladiATR attachment, or on a JASCO FT/IR-4100 Spectrometer as KBr pellets. Thermogravimetric analysis (TGA) was carried out on a TA Instruments TGA Q500. Elemental analysis was performed by Atlantic Microlabs (Norcross, GA) with CHN combustion analysis carried out on a Carlo Erba 1108 analyzer. Time-resolved emission spectroscopy (TRES) for singlet oxygen quantum yield determination was conducted on an FL/FS920 Spectrofluorimeter (Edinburgh Instruments) equipped with a 450 W Xe arc lamp.

Photosensitizer Synthesis

5-(4-nitrophenyl)-10,15,20-tris-(4-pyridyl)porphyrin (1). To a solution of 598 mL propionic acid/10% acetic anhydride were added 10 g of 4-nitrobenzaldehyde (66 mmol, 1.75 equiv) and 10.7 mL of 4-pyridinecarboxaldehyde (113 mmol, 3 equiv) with vigorous stirring at 110 °C. Next, 10.5 mL of pyrrole (151 mmol, 4 equiv) was added dropwise. After 1.75 h, the reaction mixture was removed from the heat source and allowed to stir overnight under ambient conditions. The solvent was removed under reduced pressure until approximately 50 mL remained. The remaining acid was neutralized with 1 M NaOH at 0 °C. The mixture was then filtered, and the precipitate was washed with additional 1 M NaOH (3 x 100 mL) and deionized (DI) H_2O (3 x 200 mL). The black precipitate was dried under reduced pressure overnight. To the precipitate, 500 mL of CH_2Cl_2 was added and allowed to stir for 1 h. The mixture was filtered, the filtrate was reduced in volume via rotary evaporation, and the crude was purified by flash chromatography ($CHCl_3$:MeOH; 98:2-90:10). 629 mg of purple crystalline material was collected (2.5%). TLC ($CHCl_3$:MeOH; 9:1): R_f 0.41; UV-visible (DMF) λ_{abs}, nm (ε, $mM^{-1}cm^{-1}$): 419 (175), 514 (10.8), 548 (4.1), 588 (3.6), 644 (1.9); ^{1}H-NMR (400 MHz, $CDCl_3$,) δ_{ppm}: 9.07 (d, 6H, J = 5.7 Hz, $H_{3,5\text{-pyridyl}}$), 8.88 (s, 6H, $H_{\beta\text{-pyrrolic}}$), 8.82 (d, 2H, J = 5 Hz, $H_{\beta\text{-pyrrolic}}$), 8.67 (d, 2H, J = 8.5 Hz, $H_{3,5\text{-nitrophenyl}}$), 8.40 (d, 2H, J = 8.5 Hz, $H_{2,6\text{-nitrophenyl}}$), 8.16 (d, 6H, J = 5.7 Hz, $H_{2,6\text{-pyridyl}}$), -2.91 (br s, 2H, $NH_{pyrrole}$); MALDI-TOF MS *m/z*: calc'd for $C_{41}H_{27}N_8O_2$: 663.2251 $[M+H]^+$, found 663.3428; FTIR-ATR: 1068, 1344, 1400, 1516, 1591, 3026 cm^{-1}.

5-(4-nitrophenyl)-10,15,20-tris-(4-N-methylpyridinium)porphyrin triiodide (2). Under Ar, to a 100-mL flask containing 34 mL DMF and 199 mg (300 mmol, 1 equiv) of **1** was added dropwise 0.56 mL MeI (9 mmol, 30 equiv). The reaction mixture was allowed to stir at room temperature for 24 h, after which the solvent was removed under reduced pressure until minimal amounts of DMF remained (~5 mL). The compound was purified by precipitation via addition of diethyl ether followed by isolation of the microcrystalline solid by centrifugation, affording a total of 320 mg of **2** as a dark red-brown crystalline product (98 %). UV-visible (H_2O) λ_{abs}, nm (ε, $mM^{-1}cm^{-1}$): 423 (89.4), 516, (15.8), 551 (12.5), 589 (11.0), 644 (9.6); ^{1}H-NMR (400 MHz, DMSO-d_6) δ_{ppm}: 9.48 (d, 6H, J = 6.8 Hz, $H_{3,5\text{-pyridyl}}$), 9.13 (m, 8H, $H_{\beta\text{-pyrrolic}}$), 9.01 (d, 6H, J = 6.8 Hz, $H_{2,6\text{-pyridyl}}$), 8.74 (d, 2H, J = 8.0 Hz, $H_{3,5\text{-nitrophenyl}}$), 8.52 (d, 2H, J = 8.0 Hz, $H_{2,6\text{-nitrophenyl}}$), 4.72 (s, 9H, N_{CH3}), -3.06 (br s, 2H, $NH_{pyrrole}$); FTIR-ATR: 1184, 1348, 1512, 1639, 3011, 3419 cm^{-1}.

5-(4-aminophenyl)-10,15,20-tris-(4-N-methylpyridinium)porphyrin trihydroxide (3). Under ambient conditions, 99 mg (91 μmol, 1 equiv) of 2 was dissolved in 9 mL of 6 M HCl in a 100-mL round bottom flask. A 9 mL solution of $SnCl_2\cdot 2H_2O$ (62 mg, 273 μmol, 3 equiv) in 6 M HCl was then added dropwise over 5 min. Next, 9 mL of glacial acetic acid was similarly added for homogeneity. The reaction mixture was allowed to stir for 15 h in the dark. The mixture was transferred to a 500-mL flask and 50 mL of H_2O was then introduced. The reaction was quenched with 1 M NaOH, and 56 g of Amberlite XAD-2 organic compound scavenger was added over 4 h until the solution appeared translucent, indicating nearly complete product scavenging. The resin beads were washed with H_2O (3 x 500 mL). The resin-product beads were then stirred in 200 mL of MeOH for 1 h to recover the target product. The mixture was filtered and the solvent removed under reduced pressure, yielding 48 mg (72 %) of **3**. UV-visible (H_2O) λ_{abs}, nm (ε, $mM^{-1}cm^{-1}$): 426 (82.8), 523 (7.0), 566 (4.9), 582 (4.8), 645 (1.9); ^{1}H-NMR (400 MHz, DMSO-d_6) δ_{ppm}: 9.54 (d, 6H, J = 6.4 Hz, $H_{3,5\text{-pyridyl}}$), 9.11 (m, 8H, $H_{\beta\text{-pyrrolic}}$), 9.00 (d, 6H, J = 6.4 Hz, $H_{2,6\text{-pyridyl}}$), 7.88 (d, 2H, J = 8 Hz, $H_{3,5\text{-aminophenyl}}$), 7.05 (d, 2H, J = 8 Hz, $H_{2,6\text{-aminophenyl}}$), 4.73 (s, 9H, N_{CH3}), -2.89 (br s, 2H, $NH_{pyrrole}$); LDI-TOF MS *m/z*: calc'd for $C_{44}H_{35}N_8$: 675.299 $[M-2H^+]^+$, found: 675.286; FTIR-ATR: 1066, 1249, 1394, 1635, 2987, 3674 cm^{-1}.

[5-(4-aminophenyl)-10,15,20-tris-(4-N-methylpyridinium)porphyrinato]zinc(II) triacetate (4). The metallation of **3** was performed *in situ* following its recovery from the Amberlite resin as described above. The free-based porphyrin was dissolved in 37 mL dry DMF and heated to 80 °C. A solution of 10 mL zinc acetate (104 mg, 569 μmol, 5 equiv) in MeOH was then added dropwise. After 6 h, the solvent was removed under reduced pressure, and the mixture was resuspended in 200 mL DI H_2O. To the flask, 25 g of Amberlite XAD-2 resin were added, and the mixture was further stirred for 72 h. The resin containing the final product was filtered and washed with water. The resin was resuspended in 150 mL MeOH, stirred for 2 h, and was subsequently filtered and washed with an additional 100 mL MeOH. The combined MeOH washings were reduced via rotary evaporation, yielding **4** as a dark purple-green solid (67 %). UV-visible (H_2O) λ_{abs}, nm (ε, $mM^{-1}cm^{-1}$): 437 (93.4), 565 (7.76), 613 (4.18); ^{1}H-NMR (400 MHz, DMSO-d_6) δ_{ppm}: 9.41 (d, 6H, J = 6.0 Hz, $H_{3,5\text{-pyridyl}}$), 8.98 (m, 8H, $H_{\beta\text{-pyrrolic}}$), 8.90 (d, 6H, J = 6.0 Hz, $H_{2,6\text{-pyridyl}}$), 7.82 (d, 2H, J = 7.5 Hz, $H_{3,5\text{-aminophenyl}}$), 7.00 (d, 2H, J = 7.5 Hz, $H_{2,6\text{-aminophenyl}}$), 4.70 (s, 9H, N_{CH3}); FTIR (KBr): 1185, 1455, 1526, 1636, 2362, 3424 cm^{-1}.

Cellulose Grafting Procedures

General Photosensitizer-to-NFC Grafting Procedure. A quantity of stock nanofibrillated cellulose in water was treated with 1 M NaOH for 30 min, thereby imparting swelling and ionization of its OH groups. The NFC was then filtered without washing to remove excess base. The alkali-NFC was added to a stirring solution of cyanuric chloride (20 equiv) in 130 mL acetone and stirred under ambient conditions. After 5 min, 130 mL DI water was added, and after an additional 15 s, the reaction was quenched with 130 mL 20% glacial acetic acid. The NFC-cyanuric chloride conjugate was then filtered and washed with 500 mL DI water followed by 500 mL acetone. The modified cellulose was then added to a stirring solution of PS (1 equiv) in 130 mL DMF. After 18 h, the PS-NFC was serially washed (4x) with 500 mL H_2O, 250 mL DMF, and 500 mL acetone until the eluent was colorless/PS-free. The resultant PS-NFC materials were dried under vacuum.

General Photosensitizer-to-Paper Grafting Procedure. An 11-cm diameter sheet of VWR qualitative grade 415 filter paper was alkalized in 1 M NaOH over 1 h. The paper was partially dried over a Büchner funnel to remove excess base. The alkalized paper was then placed in a solution of cyanuric chloride (20 equiv) in 50 mL acetone and manually agitated for 5 min. Then, 50 mL DI H_2O was added followed by the immediate introduction of 50 mL 20% acetic acid to quench the reaction. This activated paper sheet was washed with 100 mL H_2O and 200 mL acetone to remove any unbound cyanuric chloride. The dry sheet was submerged in a solution of PS (1 equiv) in 80 mL DMF and placed in a shaker at 150 rpm for 18-24 h in the dark. The PS-paper conjugate was repeatedly washed with DMF, H_2O, and acetone to remove excess PS. The resulting PS-paper materials were dried in the dark at 37 °C for 24 h.

Direct Metalation of A_3B^{3+}-NFC. To a round bottom flask containing 20 mL DMF was added 50 mg of **A_3B^{3+}-NFC** (5.1 μmol **3**, 1 equiv) under ambient conditions. 5.8 mg of $Zn(OAc)_2{\cdot}2H_2O$ (25.4 μmol, 5 equiv) dissolved in 5 mL DMF was then added dropwise over 1 min. After 24 h, the material was filtered, washed with 500 mL DI water, 200 mL acetone, and 500 mL water, and then dried under vacuum.

Antimicrobial Photodynamic Inactivation Studies

PDI Instrumentation. All bacteria were cultured in a VWR Incubating Mini Shaker at 350 rpm and 37 °C. A Thermo Electron Corporation Genesys 10 UV-Vis scanning spectrophotometer was used for the measurement of optical densities. Bacterial pelleting was conducted in a Thermo Electron Corporation Sorvall® Legend RT centrifuge. A LumaCare USA model LC122 PDT non-coherent light source was employed for all antimicrobial photodynamic inactivation studies. The lamp was equipped with an OSRAM 64653 HLX Xenophot bulb (250 W, 24 V), and employed a LUM V (400–700 nm band pass filter) fiber optic probe with a ~95 ± 3% average transmittance (T_{avg}). Fluence rates were measured in units of mW/cm^2 with an Ophir Orion power meter.

Bacterial Culture Conditions. Multi-drug resistant *Acinetobacter baumannii* (AB; ATCC-1605) was grown in LB-Miller broth with 5 mg/L tetracycline; methicillin-resistant *Staphylococcus aureus* (MRSA; ATCC-44) was grown in tryptic soy broth (TSB) with 5 mg/L tetracycline; *Klebsiella pneumoniae* (KP; ATCC-2146) was grown in BD Difco Nutrient Broth #234000 with 100 mg/L ampicillin; vancomycin-resistant *Enterococcus faecium* (VRE; ATCC-2320) was grown in BD Difco Bacto Brain Heart Infusion #237500 with 100 mg/L ampicillin. Bacterial strains were grown to an initial concentration of 1-5×10^8 CFU/mL; the concentration of cultures was monitored by optical density measurements at 600 nm (OD_{600}). Cultures were pelleted via centrifugation at 3716 g (4150 rpm) for 10 min, the supernatant was decanted, and the bacteria were resuspended in 5 mL of phosphate buffer saline (PBS; aqueous solution of 170 mM NaCl, 3.4 mM KCl, 10.0 mM Na_2HPO_4, 1.8 mM KH_2PO_4, pH 7.2) containing 0.05% Tween-80.

Preparation of PS-NFC Stock Suspensions. Stock suspensions of A_3B^{3+}-NFC (1 mM) and ZnA_3B^{3+}-NFC (100 μM) were prepared with ultrapure water based on molar concentrations (mol photosensitizer/g material) determined by CHN combustion analysis and maintained under dark conditions. In preparation for each suspension, the dry NFC materials were finely ground with mortar and pestle for easy mixing. Before each suspension was used in PDI experiments, the samples were vigorously vortexed to ensure homogeneity.

Bacterial Inactivation Studies. Inactivation studies were performed using sterile, flat-bottom 24-well plates (BD Falcon). For PS-paper materials, samples were cut to precisely fit the well bottom (~1 cm diam.) using a custom hole punch, whereas those performed using PS-NFC involved the resuspension of both bacteria and the respective PS-NFC stock suspension in phosphate buffer saline. Aliquots (100 μL) of resuspended cells in PBS were transferred to each well and subjected to visible (400–700 nm, 65 ± 5 mW/cm^2 fluence rate) light illumination for the indicated time period. All bacterial illumination studies were conducted in triplicate, with two dark control samples, and one material-free dark control sample taken prior to cell pelleting to verify the final growth concentration in colony forming units (CFU).

Upon the completion of the illumination period, 40 μL aliquots were taken from each of the illuminated, material-free dark control, and material-containing dark control wells, and diluted by a factor of 10 in 0.65 mL Eppendorf tubes containing 360 μL of PBS. A 1:10 serial dilution was conducted a total of six times for each sample. Each series was plated (LB-media-agar for multi-drug-resistant *A. baumannii* (MDRAB); TSB-agar for methicillin-resistant *S. aureus*; BD Difco Nutrient Broth #234000-agar for *K. pneumoniae*; BD Difco Bacto Brain Heart Infusion #237500-agar for vancomycin-resistant *E. faecium*) using gridded plates as previously published by Jett and coworkers.[64] The plates were incubated in the dark at 37

°C for a period of 15-24 h. Bacterial cell survival was quantified as a ratio of CFU/mL of the illuminated samples relative to the material-free dark controls. Representative images of illuminated vs. non-illuminated plates employed in the colony-counting method are shown in Figure S1 (Supporting Information). The highest degree inactivation detectable was limited by the plating technique employed; 6 log units of detection in CFU/mL were possible with a starting concentration of 10^8 CFU/mL. Survivability values limited to $\geq$ 0.0001% were recorded, with this value representing the detection limit. Statistical significance was assessed using an unpaired Student's two-tailed t-test.

Viral Inactivation Studies. Vero E6 cells (ATCC VERO C1008) were employed to propagate (and titer by plaque assay) vesicular stomatitis virus (VSV) NJ strain and dengue-1 virus. 25 μL of either viral stock (1×10^6 plaque forming units (PFU)/mL for VSV, and $2\text{x}10^4$ PFU/mL for dengue-1) were added to either empty well (control), PS-NFC, or PS-Pap in wells of a 96-well plate in the dark. The plates were subjected to visible (400–700 nm) light illumination as described above for the antibacterial assay, or were kept in the dark for the control experiments. Studies were performed in biological triplicates. After illumination, 100 μL of minimum essential medium (MEM) supplemented with 1% FBS, 10 mM HEPES and antibiotics were added to wash remaining viruses off the textiles. Viruses were subsequently titered by serial dilution (10-fold) using Vero cells in 12-well plates at 37 °C. Virus concentration was determined by plaque assay using crystal violet staining to visualize the plaques 24 h after infection in the case of VSV. For dengue virus, infectious foci were detected at 72h post infection by immunostaining with the mouse monoclonal pan-flavivirus specific antibody D1-4G2 and a horseradish peroxidase conjugated secondary anti-mouse antibody. Foci were visualized by incubation with the Vector VIP peroxidase substrate kit (Vector Laboratories).

Results and Discussion

Synthesis

We have previously employed the Cu(I)-catalyzed Huisgen-Meldal-Sharpless 1,3-dipolar cycloaddition, a "click reaction", for the covalent attachment of photosensitizers to cellulose.[16-18] This procedure required an extensive pretreatment protocol involving the tosylation (48 h) and azide surface modification (24 h) of the cellulose scaffolding followed by the linking of the photosensitizer (36 h). Though covalent attachment and successful microbial inactivation were observed, material production resulted in low yields with a significant amount of the photosensitizer being wasted. Moreover, that strategy was specific to a single, custom-synthesized (alkyne-bearing) photosensitizer, and cannot be extended to other commercially available ones. As a result, and inspired by the work of Sol and co-workers,[19, 20] we have shifted to a more efficient, higher yielding, and practical grafting procedure involving the use of a triazine linker, cyanuric chloride, as the means to covalently attach a porphyrin photosensitizer to cellulose,[36] thereby creating our target nanofibrillated cellulose-photosensitizer conjugate. We selected the **A_3B^{3+}** (**3**) photosensitizer here given that previous studies employing this PS and the related parent 5-10,15,20-tetrakis-(4-N-methylpyridyl)-*21H*,*23H*-porphyrin (TMPyP) strongly suggest a Type II mode of action where singlet oxygen is the dominant reactive oxygen species responsible for the inactivation of the target pathogen.[65-68]

A general route for the synthesis of the PS-NFC (**A_3B^{3+}-NFC**) and PS-paper (**A_3B^{3+}-Pap**) materials, as well as their metallated analogs, is shown in Scheme 1, and their physical appearance is shown in Figure 1. Briefly, mildly alkalized nanocellulose was treated with an excess of 2,4,6-trichloro-1,3,5-triazine, filtered to remove the unreacted coupling agent, and then reacted with 1 equiv photosensitizer, thereby yielding the desired PS-modified cellulose. When compared to the aforementioned "Click chemistry" method that required an alkyne-bearing photosensitizer and azide-functionalized cellulose fibers or nanocrystals,[16-18] this route affords several advantages: 1) no functionalization of the cellulose (i.e., with sodium azide) was needed, thus reducing the number of synthetic steps overall; 2) no heating was required, as all reactions proceeded under ambient conditions; 3) no metal-based catalyst was used; and 4) although a synthetic porphyrin was used here as the PS, the triazine-coupling method is broadly applicable to both synthetic and natural PS that contain a wide variety of nucleophilic groups. Whereas the "click reaction" route takes ~5-days, the alkalization of cellulose can be carried out over 1 h, the reaction with cyanuric chloride conducted in 10 min, and the covalent attachment of the photosensitizer in 18 h (though significant conjugation was observed within 1 h), representing a significant savings in time.

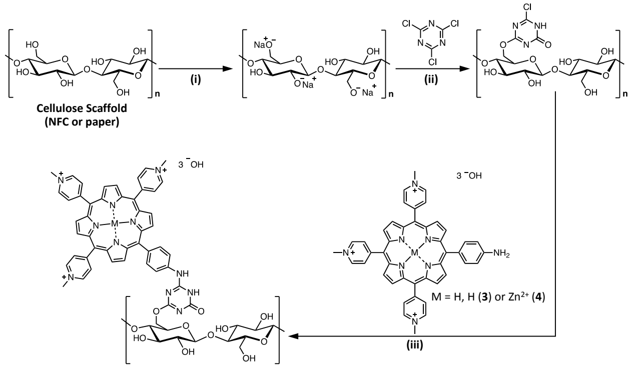

Scheme 1. Synthesis of nanofibrillated cellulose-porphyrin conjugates by 2,4,6-trichloro-1,3,5-triazine. (i) 1 M NaOH, RT, 1 h; (ii) 20 equiv. 2,4,6-trichloro-1,3,5-triazine, acetone, RT, 10 min; (iii) 1 equiv **3** or **4**, DMF, RT, 18 h.

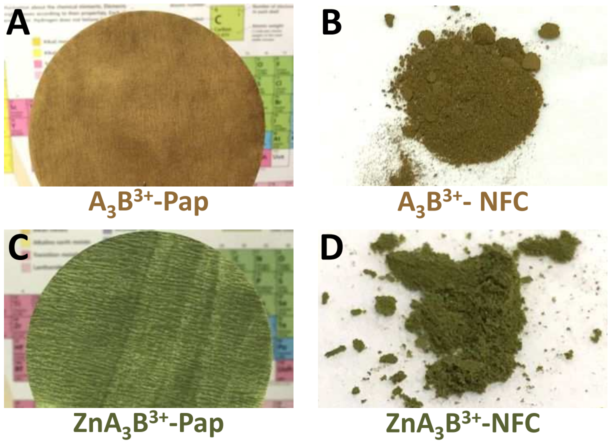

Figure 1. Photosensitizer-cellulose conjugate materials (A) A_3B^{3+}-Pap; (B) A_3B^{3+}-NFC; (C) ZnA_3B^{3+}-Pap; (D) ZnA_3B^{3+}-NFC.

Materials Characterization

Photosensitizer Loading. The nitrogen-content of **A_3B^{3+}-Pap/NFC** and **ZnA_3B^{3+}-Pap/NFC** materials was determined by elemental analysis (**Table 1**). When compared to the value for the corresponding precursor triazine-cellulose intermediate, the difference represented the level of porphyrin loading. Calculations of the wt% triazine were based on the stoichiometric molar addition of 3 nitrogen atoms to the nitrogen-free cellulose scaffolding, whereas the wt% of PS loading accounted for an additional 8 nitrogen atoms of the porphyrin photosensitizer. It was determined that the porphyrin content of **A_3B^{3+}-Paper** was 1.94 wt% (28.7 nmol/mg), **ZnA_3B^{3+}-Paper** was 1.27 wt% (17.2 nmol/mg), and **A_3B^{3+}-NFC** was 7.40 wt% (109 nmol/mg). As **ZnA_3B^{3+}-NFC** was metallated directly from the precursor **A_3B^{3+}-NFC** material, the porphyrin loading was equivalent in both materials. We surmise that the higher porphyrin loading of the NFC scaffold versus paper was due to the increased surface area of the NFC compared to the macrofibers of the cellulose paper itself. By way of comparison to previously studied PS-cellulose conjugates, Por$^{(+)}$-paper had a loading of 12.4 nmol PS/mg,[17] BC-10-PPIX had a loading of 13.0 nmol PS/mg,[61] Por$^{(+)}$-CNCs (cellulose nanocrystals) were loaded to 160 nmol PS/mg,[16] and RC-TETA-PPIX-Zn nanofibers were found to have a loading of 412 nmol PS/mg material.[60] Altogether, PS-cellulose conjugates employing nanoscale scaffolds yield PS loadings in the range of 100-400 nmol/mg, whereas those materials employing more conventional scale fibers exhibit significantly lower loading values.

Table 1. Elemental analysis (wt% N) and calculated photosensitizer loading and degree of substitution values (D. S.).

	A_3B^{3+}-Paper	ZnA_3B^{3+}-Paper	A_3B^{3+}-NFC
wt% N			
Triazine-cellulose	0.51	0.57	0.90
PS-cellulose	0.79	0.77	2.04
PS loading			
wt% PS	1.94	1.27	7.40
nmol PS/mg	28.7	17.2	109
D.S.[a]	0.0048	0.0029	0.0198

[a] D.S. = degree of substitution based on the molecular weight of the anhydroglucose unit of 162 g/mol.

Scanning Electron Microscopy. Scanning electron microscopy images were obtained on neat, freeze-dried nanofibrillated cellulose and the A_3B^{3+}-NFC conjugate to observe the morphological impacts on the nanostructure post photosensitizer affixation (Figure S2, Supporting Information). As expected, the nanoscale characteristics of the neat nanofibrillated cellulose were not preserved owing to the dehydration of the freeze-drying process under high vacuum. However, the **A_3B^{3+}-NFC** material clearly exhibited nanoscale features (pores and fibers), and we attributed this observation to the high level of cross-linking by the triazine linker that prevented the hydrogen-bonding induced collapse of the nanostructures.

UV-Visible Diffuse Reflectance Spectroscopy. UV-visible diffuse reflectance spectra were obtained for the **A_3B^{3+}-Pap/NFC** and **ZnA_3B^{3+}-Pap/NFC** conjugates and compared to their respective unbound porphyrin compounds **3** and **4** in aqueous solution (**Figure 2**). Bathochromic shifts of the Soret and Q-bands were detected in the UV-Vis DRS spectra of the **A_3B^{3+}-NFC** [436 (Soret), 526, 567, 588, 651 nm] and **A_3B^{3+}-Pap** [436 (Soret), 526, 558, 585, 651 nm] materials relative to the solution **A_3B^{3+}** porphyrin **3** [426 (Soret), 523, 566, 582, 643 nm] in H_2O (**Figure 2A**). A similar observation was made for both **ZnA_3B^{3+}-NFC** [449 (Soret), 571, 617 nm] and **ZnA_3B^{3+}-Pap** [449 (Soret), 571, 617 nm] conjugates in comparison to **ZnA_3B^{3+}** (**4**, [437 (Soret), 565, 613 nm]; **Figure 2B**). Such bathochromic shifts have been previously attributed to the differences in the local environment (e.g., polarity, solvation) of the porphyrin when covalently appended to cellulose vs. the solution spectrum.[16, 17, 60, 61] For both the PS-Pap and PS-NFC materials, the characteristic collapse of the four Q bands of the free-base porphyrin to two was noted upon metalation by zinc.[69] Finally, the presence of a small band at 525 nm in the spectrum of the **A_3B^{3+}Zn-NFC** (**Figure 2B**, black) was noted, owing to incomplete metalation of the precursor **A_3B^{3+}-NFC** that was estimated to be (<10%).

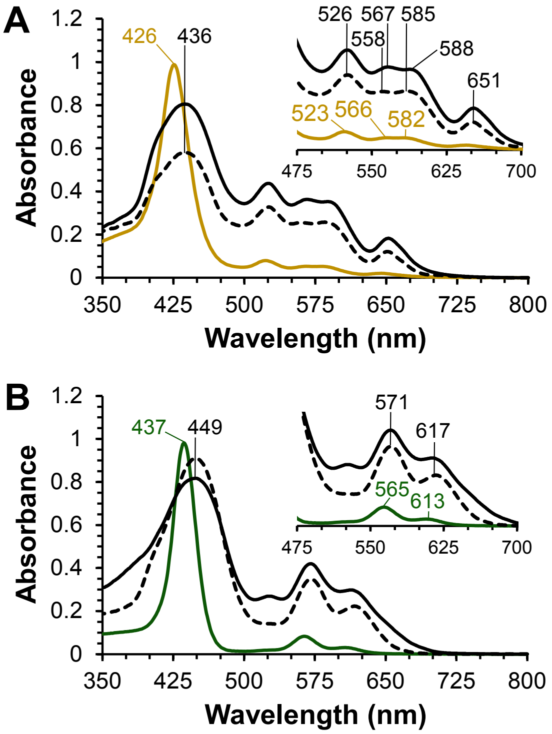

Figure 2. UV-Vis diffuse reflectance spectra of PS-cellulose conjugates. (A) **A_3B^{3+}-Pap** (dashed) and **A_3B^{3+}-NFC** (black) overlaid with the solution spectrum of **3** in H_2O (brown). (B) **A_3B^{3+}Zn-Pap** (dashed) and **A_3B^{3+}Zn-NFC** (black) overlaid with the solution spectrum of **4** in H_2O (green).

FTIR Spectroscopic Studies. Additional characterization was provided by Fourier transform infrared (FTIR) spectroscopy (**Figure 3**). Spectra were normalized to the C=O stretching band at 1060 cm^{-1}.[70] The FTIR spectrum of neat cellulose fibers confirmed several main bands characteristic of the natural polymer: 3000-3600 cm^{-1} (varied O-H stretching modes and intermolecular H-bonding), 2750-2950 cm^{-1} (C-H stretching), 1432 cm^{-1} (CH_2 bending), 1375 (C-H bending), 1060 cm^{-1} (C-O stretching).[70] The observed peak at 1630-1640 cm^{-1} is ascribed to cellulose's CH_2-O-H bending or H-O-H bending of the material's absorbed water.[71] The spectra of the triazine-cellulose intermediates revealed an additional peak between 1715-1725 cm^{-1}, indicative of amide functionalization upon the substitution of the final chlorine atom on the triazine ring. As expected, no bands of the porphyrin were observed in the PS-cellulose conjugates in accordance with the low degree of substitution (< 0.02) of the associated PS (for comparative purposes, see the Supporting Information for the ATR-IR spectra of **A_3B^{3+}** (**3**) and **ZnA_3B^{3+}** (**4**), Figure S3).

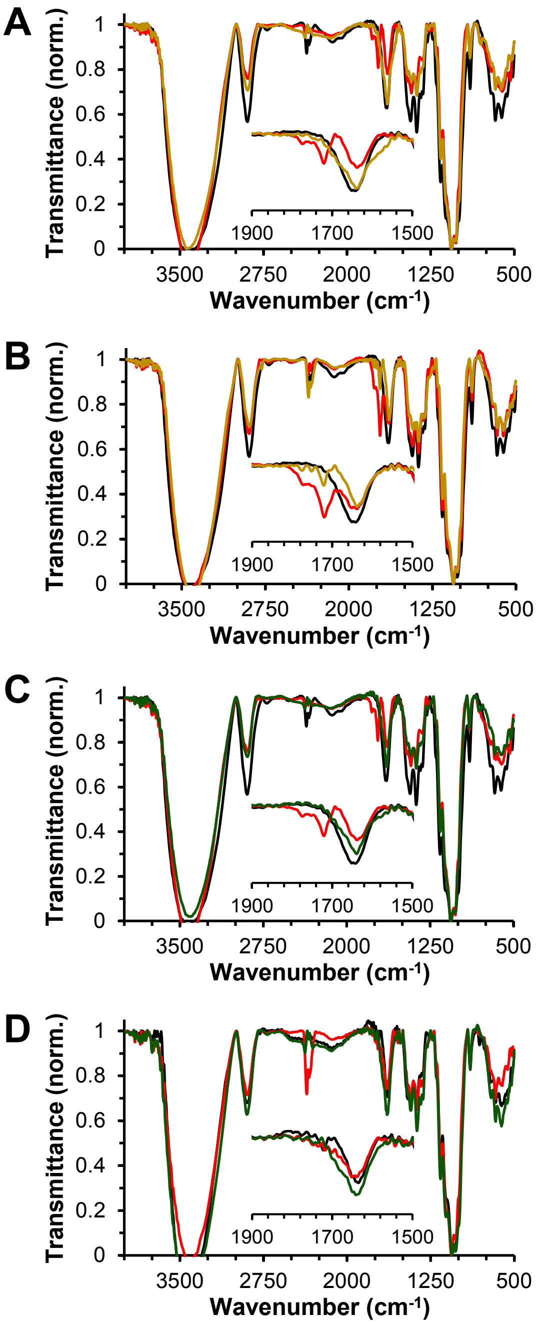

Figure 3. Fourier transform infrared spectra of (A) **A_3B^{3+}-NFC** (brown), (B) **A_3B^{3+}-Pap** (brown), (C) **ZnA_3B^{3+}-NFC** (green), and (D) **ZnA_3B^{3+}-Pap** (green). For panels A-D, the black spectra represent neat cellulose material, and the red spectra represent the triazine-cellulose intermediate.

Thermal Gravimetric Analysis. The thermal decomposition profiles of pristine cellulose, triazine-conjugate intermediates, **A_3B^{3+}-NFC/-Pap** and **ZnA_3B^{3+}-NFC/-Pap** under an inert atmosphere were investigated using thermal gravimetric analysis (**Figure 4**). In the first stage up to 100 °C, a minor initial weight loss of ~5-10% was noted for all materials, and was attributed to the loss of absorbed water. The TGA curves of pristine NFC (**Figure 4A** and **4C**) and paper (**Figure 4B** and

4D) each showed a main stage of decomposition with onset temperatures of 250 °C and 290 °C, respectively, with corresponding decomposition maxima at ca. 350 °C and 360 °C. The triazine-NFC precursor showed similar onset and decomposition maximum temperatures as pristine NFC, but with modestly greater wt % loss; however, the onset temperature (300 °C) and decomposition maximum (400 °C) were higher for triazine-paper vs. pristine paper, suggesting that intra-strand crosslinking has a more significant (and stabilizing) effect on the thermal decomposition behaviour of cellulose macrofibers than NFC. Finally, the presence of the porphyrin photosensitizer in the **A_3B^{3+}-NFC/-Pap** and **ZnA_3B^{3+}-NFC/-Pap** materials had a minor effect (± 10 °C) on the TGA profiles when compared with the precursor triazine-cellulose material. Altogether, the TGA data suggest that the covalent coupling strategy and choice of porphyrin do not negatively affect the overall thermal decomposition behavior of NFC or paper materials.

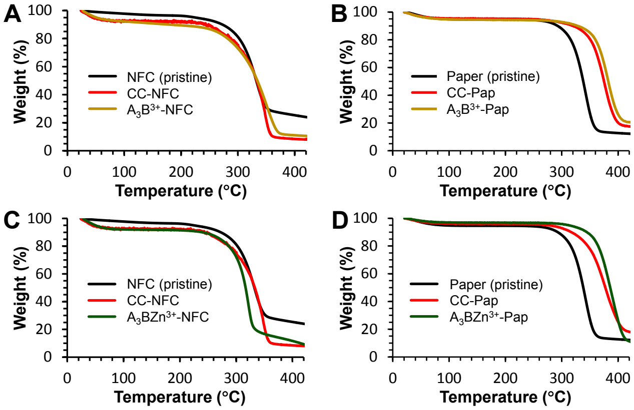

Figure 4. Thermal gravimetric analysis of A) **A_3B^{3+}-NFC**, B) **A_3B^{3+}-Pap**, C) **ZnA_3B^{3+}-NFC**, and D) **ZnA_3B^{3+}-Pap**.

Pathogen Photodynamic Inactivation Results

Antibacterial Activity of A_3B^{3+}-NFC and ZnA_3B^{3+}-NFC. Unless otherwise noted, *in vitro* aPDI assays employing the PS-cellulose conjugates were performed under fixed illumination conditions (1 h, 400–700 nm, 65 ± 5 mW/cm^2). Both the material-free dark and material-present dark controls showed no significant inactivation, demonstrating the requirement for both the photosensitizer and light for bacterial inactivation. LIVE/DEAD bacterial cell viability assays (Figure S4) further confirmed that the bactericidal activity of **A_3B^{3+}-NFC** was attributable directly to the illumination of the material. Material-free light controls have also previously shown no statistically-significant effect under the conditions examined here,[44] ruling out an antimicrobial effect by light alone. For aPDI assays employing the PS-NFC materials, concentration-dependent studies were initially performed against MRSA and MDRAB in order to determine the optimal concentration (data not shown). Against MRSA, 0.5, 2.5, 5, and 20 μM concentrations of **A_3B^{3+}-NFC** resulted in complete (6 log) reduction in the pathogen. Illumination studies against MDRAB saw complete inactivation at 20 μM (data not shown), but a decrease in performance at 5 μM, 99.9938% reduction (~4.2 log, $P = 0.004$). As a result, 5 μM was chosen as a comparative concentration between the two materials, **A_3B^{3+}-NFC** and **ZnA_3B^{3+}-NFC**.

Against two Gram-positive bacteria, methicillin-resistant *S. aureus* ATCC #BAA-44 (MRSA) and vancomycin-resistant *E. faecium* ATCC-2320 (VRE), both **A_3B^{3+}-NFC** and **ZnA_3B^{3+}-NFC** achieved detection limit inactivation (99.9999%, 6 log units reduction in CFU/mL; $P < 0.02$). Against multidrug-resistant *A. baumannii* ATCC #BAA-1605 (MDRAB), a Gram-negative bacterium, **A_3B^{3+}-NFC** achieved a 99.994% (4.5 log units, $P = 0.004$) inactivation, whereas **ZnA_3B^{3+}-NFC** reached the detection limit (99.9999%, 6 log units; $P = 0.006$). We surmise that the higher level of inactivation afforded by **ZnA_3B^{3+}-NFC** is due to a higher singlet oxygen quantum yield (Φ_Δ) of 0.156 for the parent ZnA_3B^{3+} photosensitizer compared to a value of 0.044 for A_3B^{3+} (see Table S1, Supporting Information), attributable to the heavy atom effect upon metalation. For **A_3B^{3+}-NFC**, no statistically significant inactivation of *K. pneumoniae* ATCC-2146 (KP) was observed, whereas inactivation with **ZnA_3B^{3+}-NFC** was minor, ~66% ($P = 0.006$).

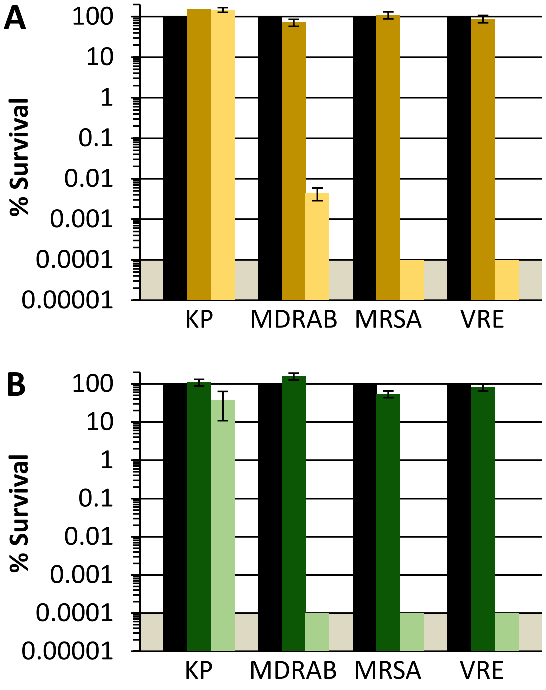

Figure 5. Photodynamic inactivation studies at 5 μM (A) **A_3B^{3+}-NFC** and (B) **ZnA_3B^{3+}-NFC** against nosocomial bacterial pathogens *K. pneumoniae* ATCC-2146 (KP), multidrug-resistant *A. baumannii* ATCC-1605 (MDRAB), methicillin-resistant *S. aureus* ATCC-44 (MRSA), and vancomycin-resistant *Enterococcus faecium* ATCC-2320 (VRE). For both panels, displayed are the material-free (cells-only) dark control set to 100% (black bars), as well as the dark controls of **A_3B^{3+}-NFC** (dark yellow) and **ZnA_3B^{3+}-NFC** (dark green), and the illuminated studies of **A_3B^{3+}-NFC** (light yellow) and **ZnA_3B^{3+}-NFC** (light green) displayed as the percent survival of the material-free dark control. For all bacteria, the illumination conditions were as follows: 60 min, 400 – 700 nm, 65 ± 5 mW/cm^2. As the plating technique employed to determine % survival did not allow for detection of survival rates of <0.0001%, data points below the detection limit were set to 0.0001% survival for graphing purposes and are indicated by the grey shaded area.

Although **ZnA_3B^{3+}-NFC** exhibited detection level photodynamic inactivation against MDRAB, MRSA and VRE that was at least comparable to, if not better than, previously studied PS-cellulose conjugates employing this photosensitizer,[16-18] the results against KP were disappointing, particularly as $Por^{(+)}$-paper was shown to inactivate this strain by 99.994+% (4.5 log units reduction).[17] We have previously observed that when using photosensitizer-modified cellulose nanocrystals, a dark pre-incubation time dependence was noted, possibly allowing for the nanoscale material to better interact with the bacteria in solution.[16, 18] To determine if such a dark incubation time-dependence was needed here with the PS-NFC to improve antimicrobial efficacy against KP, the pathogen was pre-incubated with 5 μM **A_3B^{3+}-NFC** or **ZnA_3B^{3+}-NFC** in the dark (0-60 min) at 37 °C prior to illumination (**Figure 6**). For **A_3B^{3+}-NFC**, a minor (52%) but statistically significant level of inactivation was observed with a 30 min dark pre-incubation, which increased to 94.8% (~1.3 log, $P = 0.001$) with a 60 min dark pre-incubation. For **ZnA_3B^{3+}-NFC**, a more impressive inactivation of 99.91% (~3.0 log, $P = 0.0007$) with just 5 min pre-incubation was noted, which further increased to 99.997% (~4.6 log, $P = 0.0009$), 99.998% (~4.7 log, $P = 0.004$), and 99.9994% (5.3 log, $P < 0.0001$) after 10, 30, and 60 min, respectively. These results demonstrated the ability of **ZnA_3B^{3+}-NFC** to achieve near detection limit inactivation of KP upon inclusion of a 60 min dark pre-incubation prior to visible light illumination, and compare favorably to the level of inactivation achieved in solution studies employing 5 μM **ZnA_3B^{3+}** (**4**) under identical illumination conditions (see Figure S5, Supporting Information). Moreover, these findings are consistent with the limited diffusibility of singlet oxygen in solution (<250 nm),[56, 57] and suggest (along with our previous findings with PS-modified CNCs[16, 18]) that nanoscale scaffolds require time in solution to associate with bacteria prior to photodynamic inactivation in order to achieve maximal inactivation efficacy.

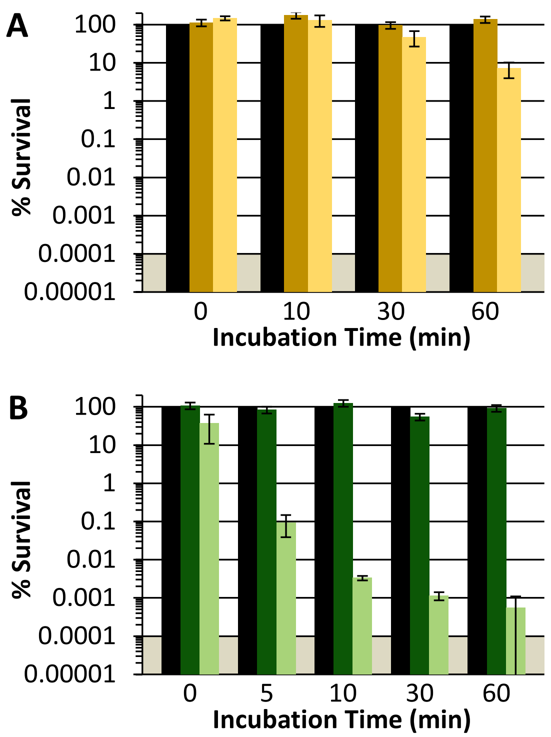

Figure 6. Photodynamic inactivation studies of *K. pneumoniae* ATCC-2146 (KP) as a function of dark pre-incubation time at 5 μM (A) **A_3B^{3+}-NFC** and (B) **ZnA_3B^{3+}-NFC**. For both panels, displayed are the material-free (cells-only) dark control set to 100%, as well as the dark controls of **A_3B^{3+}-NFC** (dark yellow) and **ZnA_3B^{3+}-NFC** (dark green), and the illuminated studies of **A_3B^{3+}-NFC** (light yellow) and **ZnA_3B^{3+}-NFC** (light green) displayed as the percent survival of the material-free dark control. The dark pre-incubation periods specified in panels A & B were performed at 37 °C in PBS. Illumination conditions and detection limits were as described in Figure 5.

Antiviral Activity of A_3B^{3+}-NFC and ZnA_3B^{3+}-NFC. Antiviral photodynamic inactivation studies employing **A_3B^{3+}-NFC** and **ZnA_3B^{3+}-NFC** at 5 μM concentration were conducted against two model enveloped viruses, vesicular stomatitis virus (VSV) and dengue-1 (**Figure 7**), using illumination conditions similar to those of the antibacterial studies (65±5 mW/cm^2, 400-700 nm, 1 h). Impressively, both materials exhibited complete (i.e., 0 PFU/mL) inactivation of the pathogens: dengue-1 by 99.99% (4-log units; **A_3B^{3+}-NFC**, $P = 0.001$; **ZnA_3B^{3+}-NFC**, $P = 0.001$), and VSV by 99.9999% (6 log units; **A_3B^{3+}-NFC**, $P = 0.001$; **ZnA_3B^{3+}-NFC**, $P < 0.0001$). Viral inactivation of ~1 log unit was also noted in the dark controls. Given the strong antiviral efficacy reported in Figure 7, we suggest that the dark inactivation resulted from the minimal light exposure needed to perform the biological assays. We note that previous photodynamic materials with strong antiviral character have also displayed 'dark' inactivation that was attributed to incidental light exposure.[17, 44, 58, 59]

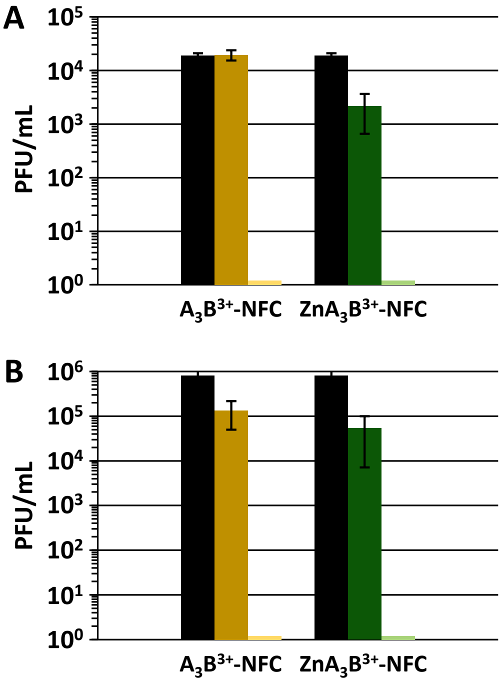

Figure 7. Photodynamic inactivation studies employing 5 μM **A_3B^{3+}-NFC** or **ZnA_3B^{3+}-NFC** against (A) dengue-1 and (B) vesicular stomatitis virus (VSV). For both panels, displayed are the material-free (cells-only) dark control set to 100%, as well as the dark controls of **A_3B^{3+}-NFC** (dark yellow) and **ZnA_3B^{3+}-NFC** (dark green), and the illuminated studies of **A_3B^{3+}-NFC** (light yellow) and **ZnA_3B^{3+}-NFC** (light green) displayed as the percent survival of the material-free dark control. Illumination conditions were as described in Figure 5. In all cases, no detectable plaque-forming units were observed, and were set to 1 PFU/mL for graphing purposes.

Antibacterial Activity of A_3B^{3+}-Pap and ZnA_3B^{3+}-Pap. Photodynamic inactivation experiments against the above nosocomial pathogens were repeated using the photosensitizer-paper conjugates, **A_3B^{3+}-Pap** and **ZnA_3B^{3+}-Pap** (**Figure 8**). The conditions were maintained consistent with the PS-NFC studies at an illumination intensity 65±5 mW/cm^2 and a wavelength range of 400-700 nm for 1 h. The freebase porphyrin-containing material, **A_3B^{3+}-Pap** (**Figure 8A**), saw a 99.9999% (VRE, P = 0.0008; MRSA, P < 0.0001; MDRAB, P < 0.0001) inactivation of VRE, MRSA, and MDRAB, and a 99.9994% (∼5.3 log, P < 0.0001) inactivation of KP. The metallated counterpart, **ZnA_3B^{3+}-Pap** (**Figure 8B**) similarly achieved detection-level inactivation of MDRAB, MRSA, and VRE, (MDRAB, P = 0.001; MRSA, P = 0.002; VRE, P = 0.002) but a slightly lower inactivation of 99.47% (∼2.3 log, P < 0.0001) against KP. This drop in antimicrobial efficacy against KB from **A_3B^{3+}-Pap** to **ZnA_3B^{3+}-Pap** is counter to the observations of the solution PS and NFC-based studies, both of which showed a higher level of inactivation for the metallated analogue. We suggest that this decrease in inactivation is more likely attributable to the lower photosensitizer loading in **ZnA_3B^{3+}-Pap** (1.27 wt%) compared with **A_3B^{3+}-Pap** (1.94 wt%). Gratifyingly, an approximately ∼2 log unit improvement (99.996%, P = 0.0003) in antibacterial efficacy against KP was observed for **ZnA_3B^{3+}-Pap** when including a dark pre-incubation of 1 hr prior to light illumination (data not shown), consistent with the pre-incubation-dependent increase in aPDI efficacy noted for the NFC-based materials.

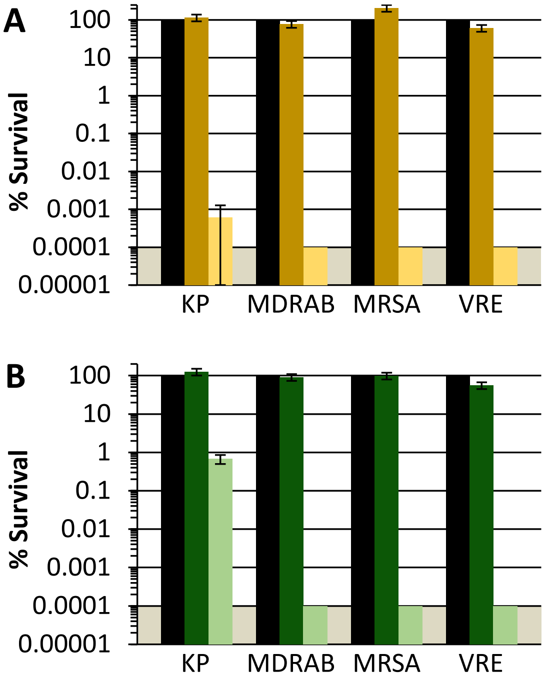

Figure 8. Photodynamic inactivation studies employing (A) **A_3B^{3+}-Pap** and (B) **ZnA_3B^{3+}-Pap** against nosocomial bacterial pathogens *K. pneumoniae* ATCC-2146 (KP), multidrug-resistant *A. baumannii* ATCC-1605 (MDRAB), methicillin-resistant *S. aureus* ATCC-44 (MRSA), and vancomycin-resistant *Enterococcus faecium* ATCC-2320 (VRE). For both panels, displayed are the material-free (cells-only) dark control set to 100% (black bars), as well as the dark controls of **A_3B^{3+}-Pap** (dark yellow) and **ZnA_3B^{3+}-Pap** (dark green), and the illuminated studies of **A_3B^{3+}-Pap** (light yellow) and **ZnA_3B^{3+}-Pap** (light green) displayed as the percent survival of the material-free dark control. Illumination conditions and detection limits were as described in Figure 5.

Conclusions

In conclusion, we have shown the synthesis, characterization, and photodynamic inactivation of photosensitizer-conjugated nanofibrillated cellulose and cellulose sheets. The triazine linker conjugation strategy, complemented by the extensive surface area of NFC, proved to be an excellent combination: the facile and relatively fast synthesis led to PS-NFC materials that demonstrated the successful inactivation of a variety of pathogenic species spanning antibiotic-resistant Gram-negative and Gram-positive bacterial strains, and two viral species. We attributed these high levels of photodynamic inactivation to the high photosensitizer loading that was achievable through the use of the nanofibrillated scaffold. Although cellulose nanocrystals (CNCs) have also demonstrated a high PS-loading, the scalability of NFC and lack of harsh acid treatment that is required for CNC production suggest that nanofibrillated cellulose is a preferred scaffold from which to design future PS-cellulose conjugates. Moreover, although we employed a synthetic and custom porphyrin in this present study, the triazine coupling strategy is amenable for use with a large variety of both commercially available (i.e., thionine) or natural (i.e., PPIX, hypocrellin) photosensitizers, and will incorporated into future iterations of these materials. Taken together, this scalable conjugation strategy has the potential to be used on bulk, nanocellulosic materials that may later be woven into a wide variety of textiles for their use in the prevention of nosocomial infections.

Conflicts of interest

There are no conflicts to declare.

Acknowledgements

This research was supported in part by a Biotechnology Innovation Grant (2016-BIG-6537) from the North Carolina Biotechnology Center, a 2016 NC State University Chancellor's Innovation Funds award, and an Air Force Institute of Technology fellowship awarded to D.R.A.

References

1 D. P. Nicolau, *Curr. Opin. Infect. Dis.*, 2011, **24 Suppl 1**, S1-10.
2 World Health Organization, *WHO Priority Pathogens List for R&D of New Antibiotics*, 2017.
3 A. Kramer, I. Schwebke and G. Kampf, *BMC Infect. Dis.*, 2006, **6**, 130.
4 J. A. Otter, S. Yezli, J. A. G. Salkeld and G. L. French, *Am. J. Infect. Control*, 2013, **41**, S6-S11.
5 A. Mariscal, R. M. Lopez-Gigosos, M. Carnero-Varo and J. Fernandez-Crehuet, *Eur. J. Clin. Microbiol. Infect. Dis.*, 2011, **30**, 227-232.
6 J. V. McArthur, R. C. Tuckfield and C. Baker-Austin, *Handb. Exp. Pharmacol.*, 2012, 135-152.
7 D. S. Morais, R. M. Guedes and M. A. Lopes, *Materials (Basel)*, 2016, **9**.
8 M. Heide, U. Mohring, R. Hansel, M. Stoll, U. Wollina and B. Heinig, *Curr. Prob.l Dermatol.*, 2006, **33**, 179-199.
9 Z. U. Iyigundogdu, O. Demir, A. B. Asutay and F. Sahin, *Appl. Biochem. Biotechnol.*, 2017, **181**, 1155-1166.
10 W. Chen, W. Wang, X. Ge, Q. Wei, R. A. Ghiladi and Q. Wang, *Fiber Polym.*, 2018, **19**, 1687-1693.
11 L. Lin, H. Cui, H. Zhou, X. Zhang, C. Bortolini, M. Chen, L. Liu and M. Dong, *Chem. Commun.*, 2015, **51**, 2653-2655.
12 M. Rose and R. Palkovits, *Macromol. Rapid Commun.*, 2011, **32**, 1299-1311.
13 Y. Habibi, L. A. Lucia and O. J. Rojas, *Chem. Rev.*, 2010, **110**, 3479-3500.
14 K. Missoum, M. N. Belgacem and J. Bras, *Materials (Basel)*, 2013, **6**, 1745-1766.
15 D. Klemm, B. Heublein, H. P. Fink and A. Bohn, *Angew. Chem.*, 2005, **44**, 3358-3393.
16 E. Feese, H. Sadeghifar, H. S. Gracz, D. S. Argyropoulos and R. A. Ghiladi, *Biomacromolecules*, 2011, **12**, 3528-3539.
17 B. L. Carpenter, F. Scholle, H. Sadeghifar, A. J. Francis, J. Boltersdorf, W. W. Weare, D. S. Argyropoulos, P. A. Maggard and R. A. Ghiladi, *Biomacromolecules*, 2015, **16**, 2482-2492.
18 B. L. Carpenter, E. Feese, H. Sadeghifar, D. S. Argyropoulos and R. A. Ghiladi, *Photochem. Photobiol.*, 2012, **88**, 527-536.
19 C. Ringot, V. Sol, M. Barriere, N. Saad, P. Bressollier, R. Granet, P. Couleaud, C. Frochot and P. Krausz, *Biomacromolecules*, 2011, **12**, 1716-1723.
20 J. P. Mbakidi, K. Herke, S. Alves, V. Chaleix, R. Granet, P. Krausz, S. Leroy-Lhez, T. S. Ouk and V. Sol, *Carbohydr. Polym.*, 2013, **91**, 333-338.
21 W. K. Son, J. H. Youk and W. H. Park, *Carbohydr. Polym.*, 2006, **65**, 430-434.
22 J. Li, Y. Liu, Z. Jiang, K. Ma, X. Ren and T.-s. Huang, *Ind. Eng. Chem. Res.*, 2014, **53**, 13058-13064.
23 R. Li, Q. Jiang, X. Ren, Z. Xie and T.-S. Huang, *J. Ind. Eng. Chem.*, 2015, **27**, 315-321.
24 S. Saini, N. Belgacem, J. Mendes, G. Elegir and J. Bras, *ACS Appl. Mater. Interfaces*, 2015, **7**, 18076-18085.
25 S. C. M. Fernandes, P. Sadocco, A. Alonso-Varona, T. Palomares, A. Eceiza, A. J. D. Silvestre, I. Mondragon and C. S. R. Freire, *ACS Appl. Mater. Interfaces*, 2013, **5**, 3290-3297.
26 T. Zhao, G. Sun and X. Song, *J. Appl. Polym. Sci.*, 2008, **108**, 1917-1923.
27 F. Le Guern, T.-S. Ouk, K. Grenier, N. Joly, V. Lequart and V. Sol, *J. Mater. Chem. B*, 2017, **5**, 6953-6962.
28 X. Qiu and S. Hu, *Materials (Basel)*, 2013, **6**, 738-781.
29 A. H. Tayeb, E. Amini, S. Ghasemi and M. Tajvidi, *Molecules*, 2018, **23**.
30 E. A. Hassan and M. L. Hassan, *Ind. Crop Prod.*, 2016, **93**, 142-151.
31 P. Bober, J. Liu, K. S. Mikkonen, P. Ihalainen, M. Pesonen, C. Plumed-Ferrer, A. von Wright, T. Lindfors, C. Xu and R. M. Latonen, *Biomacromolecules*, 2014, **15**, 3655-3663.
32 N. C. T. Martins, C. S. R. Freire, R. J. B. Pinto, S. C. M. Fernandes, C. Pascoal Neto, A. J. D. Silvestre, J. Causio, G. Baldi, P. Sadocco and T. Trindade, *Cellulose*, 2012, **19**, 1425-1436.
33 I. Díez, P. Eronen, M. Österberg, M. B. Linder, O. Ikkala and R. H. A. Ras, *Macromol. Biosci.*, 2011, **11**, 1185-1191.
34 N. C. T. Martins, C. S. R. Freire, C. P. Neto, A. J. D. Silvestre, J. Causio, G. Baldi, P. Sadocco and T. Trindade, *Colloids Surf. Physicochem. Eng. Aspects*, 2013, **417**, 111-119.
35 K. Littunen, J. Snoei de Castro, A. Samoylenko, Q. Xu, S. Quaggin, S. Vainio and J. Seppälä, *Eur. Polym. J.*, 2016, **75**, 116-124.
36 J. Warren, J. D. Reid and C. Hamalainen, *Text. Res. J.*, 1952, **22**, 584-590.
37 Z. J. Kamiński, *Synthesis*, 1987, **1987**, 917-920.
38 T. Carofiglio, M. Schiorlin and U. Tonellato, *J. Porphyrins Phthalocyanines*, 2007, **11**, 749-754.
39 J. T. Thurston, J. R. Dudley, D. W. Kaiser, I. Hechenbleikner, F. C. Schaefer and D. Holm-Hansen, *J. Am. Chem. Soc.*, 1951, **73**, 2981-2983.

40 K. M. Al-Zaydi, H. H. Khalil, A. El-Faham and S. N. Khattab, *Chem. Cent, J.*, 2017, **11**, 39.

41 M. R. Hamblin, *Curr. Opin. Microbiol.*, 2016, **33**, 67-73.

42 E. Feese and R. A. Ghiladi, *J. Antimicrob. Chemother.*, 2009, **64**, 782-785.

43 T. Ito and K. Kobayashi, *Photochem. Photobiol.*, 1977, **25**, 399-401.

44 B. L. Carpenter, X. Situ, F. Scholle, J. Bartelmess, W. W. Weare and R. A. Ghiladi, *Molecules*, 2015, **20**, 10604-10621.

45 L. Sobotta, P. Skupin-Mrugalska, J. Mielcarek, T. Goslinski and J. Balzarini, *Mini-Rev. Med. Chem.*, 2015, **15**, 503-521.

46 T. Dai, B. B. Fuchs, J. J. Coleman, R. A. Prates, C. Astrakas, T. G. St Denis, M. S. Ribeiro, E. Mylonakis, M. R. Hamblin and G. P. Tegos, *Front. Microbiol.*, 2012, **3**, 120.

47 L. Costa, M. A. Faustino, M. G. Neves, A. Cunha and A. Almeida, *Viruses*, 2012, **4**, 1034-1074.

48 Q. Chen, L. Zhang, Y. Feng, F. Shi, Y. Wang, P. Wang and L. Liu, *J. Mater. Chem. B*, 2018, **6**, 7643-7651.

49 Y. Feng, L. Liu, J. Zhang, H. Aslan and M. Dong, *J. Mater. Chem. B*, 2017, **5**, 8631-8652.

50 J. Zhang, Y. Feng, J. Mi, Y. Shen, Z. Tu and L. Liu, *J. Hazard. Mater.*, 2018, **342**, 121-130.

51 Y. Feng, Q. Chen, Q. Yin, G. Pan, Z. Tu and L. Liu, *ACS Appl. Bio Mater.*, 2019, **2**, 747-756.

52 A. Tavares, C. M. Carvalho, M. A. Faustino, M. G. Neves, J. P. Tome, A. C. Tome, J. A. Cavaleiro, A. Cunha, N. C. Gomes, E. Alves and A. Almeida, *Mar. Drugs*, 2010, **8**, 91-105.

53 S. P. Tseng, L. J. Teng, C. T. Chen, T. H. Lo, W. C. Hung, H. J. Chen, P. R. Hsueh and J. C. Tsai, *Lasers Surg. Med.*, 2009, **41**, 391-397.

54 D. M. Vera, M. H. Haynes, A. R. Ball, T. Dai, C. Astrakas, M. J. Kelso, M. R. Hamblin and G. P. Tegos, *Photochem. Photobiol.*, 2012, **88**, 499-511.

55 F. Giuliani, M. Martinelli, A. Cocchi, D. Arbia, L. Fantetti and G. Roncucci, *Antimicrob. Agents Chemother.*, 2010, **54**, 637-642.

56 P. B. Merkel and D. R. Kearns, *J. Am. Chem. Soc.*, 1972, **94**, 7244-7253.

57 W. R. Midden and S. Y. Wang, *J. Am. Chem. Soc.*, 1983, **105**, 4129-4135.

58 B. S. T. Peddinti, F. Scholle, R. A. Ghiladi and R. J. Spontak, *ACS Appl. Mater. Interfaces*, 2018, **10**, 25955-25959.

59 S. Stanley, F. Scholle, J. Zhu, Y. Lu, X. Zhang, X. Situ and R. Ghiladi, *Nanomaterials*, 2016, **6**, 77.

60 J. Dong, R. A. Ghiladi, Q. Wang, Y. Cai and Q. Wei, *Nanotechnology*, 2018, **29**, 265601.

61 J. Dong, R. A. Ghiladi, Q. Wang, Y. Cai and Q. Wei, *Cellulose*, 2018, **25**, 1673-1686.

62 Y. Su, J. Sun, S. Rao, Y. Cai and Y. Yang, *J. Photochem. Photobiol. B: Biol.*, 2011, **103**, 29-34.

63 M. A. Paschoal, C. C. Tonon, D. M. P. Spolidório, V. S. Bagnato, J. S. M. Giusti and L. Santos-Pinto, *Photodiagn. Photodyn. Ther.*, 2013, **10**, 313-319.

64 K. L. H. Bradley D. Jett, Mark M. Huycke, and Michael S. Gilmore, *BioTechniques*, 1997, **23**, 648-650.

65 F. Le Guern, V. Sol, C. Ouk, P. Arnoux, C. Frochot and T.-S. Ouk, *Bioconjugate Chem.*, 2017, **28**, 2493-2506.

66 D. B. Eckl, L. Dengler, M. Nemmert, A. Eichner, W. Bäumler and H. Huber, *Photochem. Photobiol.*, 2018, **94**, 165-172.

67 P. Henke, K. Lang, P. Kubat, J. Sykora, M. Slouf and J. Mosinger, *ACS Appl. Mater. Interfaces*, 2013, **5**, 3776-3783.

68 M. Salmon-Divon, Y. Nitzan and Z. Malik, *Photochem. Photobiol. Sci.*, 2004, **3**, 423-429.

69 J. E. Falk, *Porphyrins and Metalloporphyrins: Their General, Physical and Coordination Chemistry, and Laboratory Methods*, Elsevier, Amsterdam, 1964.

70 M. Kačuráková, A. C. Smith, M. J. Gidley and R. H. Wilson, *Carbohydr. Res.*, 2002, **337**, 1145-1153.

71 C. J. Huntley, K. D. Crews and M. L. Curry, *Int. J. Polym. Sci.*, 2015, **2015**, 9.

72

Table of Contents Entry

Anti-infective materials based upon renewable nanocellulose-porphyrin conjugates photodynamically inactivated four strains of drug-resistant bacteria and two viruses by 99.999+%.